

Atmospheric Corrosion Behaviour of Benzotriazole Treated Cu-based Coins in Synthetic Sweat

Songpeng Huang^{1,2}, Xuexin Song^{1,2}, Chen Pan^{1,2}, Gongwang Cao^{1,2}, Zhenyao Wang^{1,2,*}

¹ School of Material Science and Engineering, University of Science and Technology of China, Shenyang 110016, China

² Institute of Metal Research, China Academy of Sciences, Shenyang 110016, China

*E-mail: zhywang@imr.ac.cn

Received: 12 March 2020 / Accepted: 5 May 2020 / Published: 10 July 2020

The atmospheric corrosion behavior of benzotriazole treated Cu-based coins in synthetic sweat was investigated. Electrochemical impedance spectroscopy showed that the protective effect of BTA on copper coins gradually failed in synthetic sweat with the prolongation of immersion time. The copper coin coated with BTA protective film had a faster corrosion rate under cyclic wet-dry test of regularly wetting synthetic sweat. From the composition analysis of protective film and corrosion products, BTA not only complexed with $\text{Cu}^{2+}/\text{Cu}^+$, but also reacted with $\text{Zn}^{2+}/\text{Ni}^{2+}$. The thickness of the patina layer can reach to 100 μm after 240h accelerated experiment, and the corrosion products were simple in composition, mainly basic $\text{Cu}_2(\text{OH})_3\text{Cl}$ and oxides of Ni and Zn. However, BTA had little protective effect on copper in synthetic sweat, and didn't affect the composition of final corrosion products.

Keywords: Copper coins; Wet-Dry cyclic; synthetic sweat; BTA (Benzotriazole)

1. INTRODUCTION

The coin occupies an important position in the long monetary history, and develops with other forms of currency. It possesses nature of medium, as a companion in the process of society economic development and trade, and has witnessed the progress of productive forces. Copper coins, as the earliest metal currency, have been used up to now with many advantages: low cost, good color and fine abrasiveness. However, copper coins are also prone to corrosion influenced by the surrounding environment. The earliest study of copper coins corrosion can be traced to bronze[1] and then brass[2]. Moreover, these copper coins are more cultural relics unearthed with the tombs[3], involving corrosion in the soil environment or closed water environment.

But for modern copper coins, corrosion in soil and underwater environment is not a common condition. The main corrosion process comes from the influence of circulation environment. It comprises

a complex physical and chemical process between external environment and the surface of copper coins, involving wet-dry alternating process and chemical reaction. The related factors include temperature, humidity, sweat and atmospheric composition (CO_2 , SO_2). Most of these factors causing the corrosion are unavoidable[4]. With regard to corrosion of copper, nickel and zinc based alloys in synthetic sweat, there were some amusing phenomenon found by Colin et al. The corrosion product of alloys with a high Cu content was mainly composed of copper(I) oxide containing chloride anions. As for alloys with a high Ni content, the corrosion layer included $\text{Cu}_2(\text{OH})_3\text{Cl}$ and Ni-compounds ($\text{Ni}(\text{OH})_2$, NiO) [5]. Therefore, a common way to prevent copper coins from corrosion is to form a protective film on its surface which can prolong the service time[6]. Considering the source of raw materials and treatment cost, BTA and its derivatives are undoubtedly the most widely used in terms of inhibiting discoloration effect in the organic inhibitor system. Chen et al.[7] reported that BTA can interact with Cu to form protective film and generated a thick polymeric $[\text{Cu}^+\text{BTA}]_n$ on the Cu_2O substrate in defect sites. While many researches are about the interaction between sweat and metals, there are less relevant literatures on effect of BTA on copper coins under sweat condition.

The purpose of this research is to analyze the corrosion behavior of BTA treated copper coins coated in a synthetic sweat by weight gain measurement, EIS measurement, SEM and XPS, and discuss the corrosion mechanism.

2. EXPERIMENTAL

2.1 Sample and solution preparations

The production process of the coin ($m=9.3\text{g}-9.7\text{g}$, $\Phi 18.7\text{mm}\times 2\text{ mm}$) was shown in Fig.1a. Only the front part of copper coins was selected as the experimental surface. Besides, in order to analyze the protective performance of BTA on copper coins in synthetic sweat, two group tests were set up: the group A without coating and the group B with coating. Samples were cleaned in alcohol, dried by cold air, and placed in a desiccator before use.

Chemical reagents were purchased from Sinopharm chemical reagent Co. Ltd (Shanghai, China). In the process of BTA treatment, Coins were immersed in inhibition solution for a period of time (20-30min, $50\text{ }^\circ\text{C}$). The basic components of the inhibition solution consisted of: 0.05 mol/L BTA(A.R.), 50 ml/L $\text{C}_2\text{H}_5\text{OH}$ (C.P.) and 0.86 mmol/L SDBS(sodium dodecyl benzene sulfate, A.R.)[8]. As the main inhibitor, BTA can react with Cu to form complex protective film. The role of ethanol was to promote the dissolution of BTA and the existence of sodium dodecyl sulfate was conducive to forming a complete film. As corrosion medium, synthetic sweat (20g/L NaCl, 17.5g/L NH_4Cl , 5g/L urea, 15g/L racemic lactic acid, 2.5g/L acetic acid, which was alkalified with sodium hydroxide to PH 4.7) was prepared from reagent-grade chemicals according to the national standard ISO 3160-2:2015[9].

Table 1. chemical composition of the copper coin (wt%)

Elements	Cu	Zn	Ni	Mn	Fe	Sn
Composition(wt%)	66.7	18.6	14.7	0.100	0.100	-

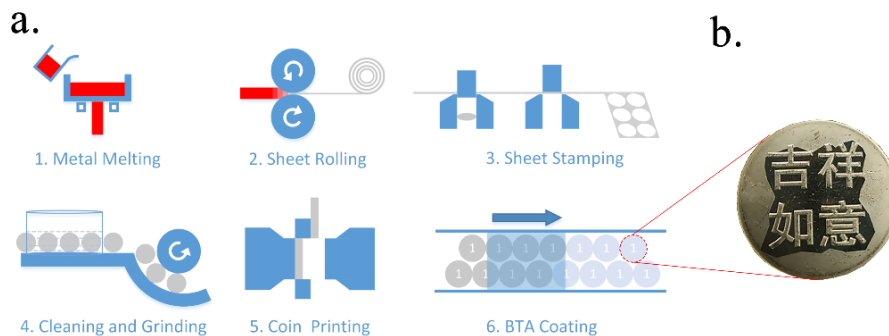


Figure 1. (a)Flow chart of coin's production and (b) Morphological details

2.2 Electrochemical measurements

The electrochemical measurements were measured by a PARSTAT 2273 workstation controlled by PowerSuite software. Platinum plate, saturated calomel electrode(SCE) and copper coin served as the counter electrode, reference electrode and working electrode respectively, in a three-electrode corrosion cell at room temperate. For the electrochemical measurement, all the coins were sealed with a mixture of paraffin and rosin, leaving an exposed working area of $1\sim 1.6\text{cm}^2$ measured by graphics software after setting up scale.

The test solution used in electrochemical measurement was synthetic sweat. Prior to electrochemical measurements, the samples were immersed in solution for 30-60min to ensure a stable open circuit potential. Then, the electrochemical impedance spectroscopy(EIS) was measured. The amplitude of the AC voltage was 10mv and the frequency range was from 10^5 Hz to 10^{-2} Hz. Because of the possible incertitude of corrosion measurements, three parallel samples were used for each group for all electrochemical measurements.

2.3 Wet-Dry cyclic corrosion test

Wet-dry cyclic corrosion tests were carried out on the samples by a Weiss-Voetsch temperature and climate test system. It involved several steps within a period of 24h: (1) weighting the initial sample, (2) smearing synthetic sweat of $1.8\mu\text{l}\cdot\text{cm}^{-2}\cdot\text{d}^{-1}$ on the sample surface, (3) drying the sample in a chamber at room temperature, (4) wetting samples in the test instrument set at 30°C and RH of 90% for 2 hours, (5) drying of the sample again in the test instrument maintained at 30°C and RH of 60% for 2 hours, and (6) steps (4) and (5) were repeated six times. The total corrosion time was 240 hours.

2.4 Characterization techniques

The corrosion products scraped off from the corroded sample were analyzed by X-ray Diffraction (XRD) to determine their phases. The XRD patterns were obtained using X'Pert-PRO diffractometer (Cu K α radiation at 40 kV) with a $2.0^\circ/\text{min}$ scanning speed and a $10\text{--}90^\circ$ of 2θ range.

The surface and cross-sectional morphologies of the corrosion products were observed by Scanning Electron Microscopy (SEM) equipped with energy dispersive spectroscopy(EDS) the FEI Quanta 450. The samples used in the observation of cross-sectional morphologies were embedded in the epoxy resin.

XPS analysis was performed using a VG ESCALAB 250 X-ray photoelectron spectrometer. The photoelectrons were excited with Al K α ($h\nu=1486.6$ eV) X-ray source and the analyzer pass energy was 50.0 eV. In addition, a delocalized Ar⁺ ion beam, accelerated under 3 kV, is used to remove contaminants on the surface ($2 \mu\text{A}/\text{cm}^2$ current density). XPS spectra are recorded in direct N(E_k) mode (E_k: Kinetic energy of the emitted photo-electron). Surface and bulk atomic concentrations are determined from the peak areas using the atomic sensitivity factor[10]. Binding energies (BEs) were calibrated against the surface carbon contamination at 284.5 eV[11-12].

3. RESULTS AND DISCUSSION

3.1 Corrosion kinetics

When all corrosion products are attached to the metal surface, or when all corrosion products fallen off can be collected, it is feasible to characterize the corrosion kinetics of metals by corrosion weight gain and the corrosion rate can be expressed by the following formula:

$$V_p = \Delta w/t \quad (1)$$

where V_p is corrosion rate ($\text{g}\cdot\text{m}^{-2}\cdot\text{h}^{-1}$), Δw is weight gain($\text{g}\cdot\text{m}^{-2}$) and t is corrosion time(h)

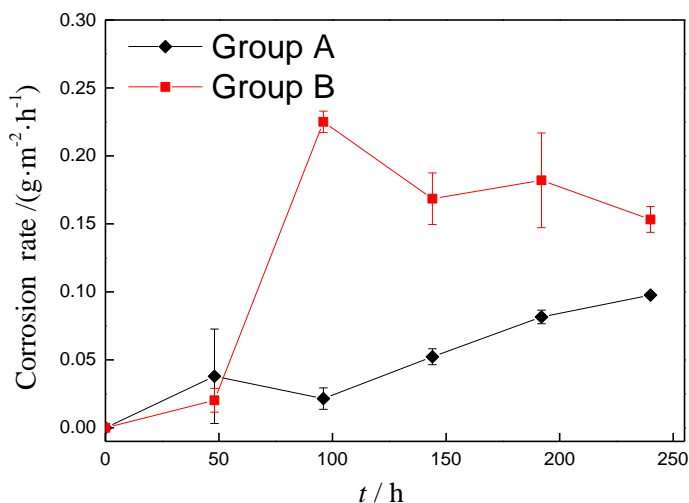


Figure 2. The average corrosion rate of copper coin coated with synthetic sweat as a function of time under wet/dry accelerated environment (group A without BTA, group B with BTA)

As some corrosion products of copper are water-soluble and cannot be washed directly with water, weight gain results may include the mass of unconsumed salt. Even so, the corrosion rate calculated by weight gain can be used to characterize the degree of the corrosion because the amount of

stimulated sweat coated is constant. Fig.2 presents copper coins' average corrosion rate all gradually tends to be gentle with the extension of time, indicating that corrosion products on metal surface reach a stable level. There is an intersection point on the curve near 48h, but the physical meaning of this region is not clear for a large error range of group A. After 60h, there is an apparent difference among two curves. The corrosion rate of group B is much higher than that of Group A. BTA may make contribution to the difference of corrosion kinetics curves between two kinds of copper coins. The protective mechanism of BTA is the formation of chemical bonds with metals or metal oxides, especially Cu-N bond[13], which results in the formation of complexes. Considering that the synthetic sweat is a kind of acidic medium containing Cl^- , it can be speculated that BTA complexes will adsorb more corrosive medium surrounding and deposit on the metal surface which facilitate the occurrence of corrosion.

3.2 Electrochemical characterization

EIS of copper coins have been measured after 2 weeks of continuous immersion in the synthetic sweat. Figure.3 shows EIS profiles of BTA-uncoated copper coins as a function of immersion time in synthetic sweat. Similar to the EIS curve for Cu in chloride solution[14-16]. The apparent presence of a 'tail' in the low frequency region corresponds to the Warburg impedance. It indicates the existence of a diffusion-controlled corrosion process on copper coins' surface, including the anodic diffusion process of soluble copper species from the surface to the bulk solution along with the cathodic diffusion of dissolved oxygen in the opposite directions. With immersion time prolonged, the Warburg impedance disappeared and the medium to high frequency limits of impedance progressively decreased within 5 d. Corrosive micro-batteries were formed at the interface between metal and solution, and the corrosion reaction was accelerated[17]. While the impedance in the low frequency region increased quickly after 7 d, it implied that the protective corrosion products were formed on the copper surface. The bode plots in Fig.3 presented two time constant clearly at the latter stages verifying corrosion process had a notable change.

Compared with group A at 0d, Figure.4 shows a larger arc of capacitive resistance from Nyquist plots of BTA-coated copper coins. The Bode plot has a wide range of phase angles, which is characterized by high impedance modulus. Therefore, the BTA film on the surface of copper coins corresponds to an insulating layer with large resistance and small capacitance[18]. During 0 to 5 d, the impedance of copper coin coated with BTA decreased gradually with immersion time. These changes indicated that the electrolyte solution slightly penetrated the substrate through the film to destroy the bonding between the protective film and the metal matrix. A similar phenomenon was reported by Zerjav et al. The BTA film formed on Cu disappeared after 24 h immersion in a simulated acidic media[19].

On the 9th day, it plainly exhibited two time constants. EIS measurement sensitively showed the process of interfacial damage of the film. The electrolyte solution markedly seeped into interface of the protective film/matrix and formed corrosive micro-batteries at the interface. In addition, the time constant corresponding to the high frequency area came from the contribution of the film capacitance, and the polarization resistance of the matrix metal reaction generated the time constant of the low

frequency region[20]. When the permeation of electrolyte solution to the membrane reached equilibrium (11-13 d), the corresponding impedance modulus at the high-frequency domain of Bode diagram did not move with the prolongation of immersion time, but appeared in the form of overlap.

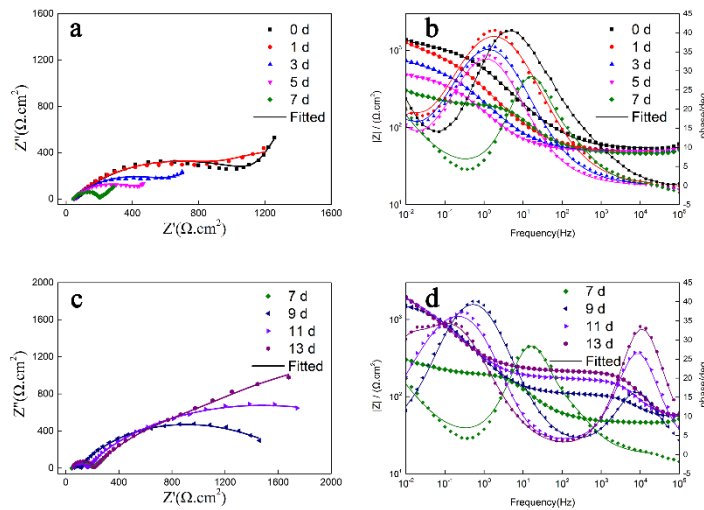


Figure 3. Nyquist(a、c) and Bode(b、d) plots for BTA-uncoated copper coins(group A) in synthetic sweat measured after 2 weeks immersion

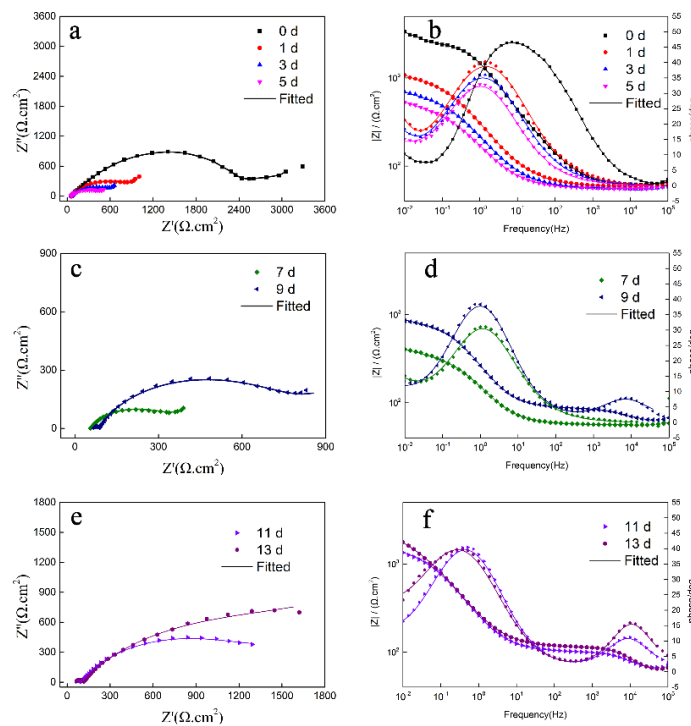


Figure 4. Nyquist(a、c、e) and Bode(b、d、f) plots for BTA-coated copper(group B) coins in synthetic sweat measured after 2 weeks immersion

The EIS data was fitted by two equivalent electrical circuits. Here, Fig.5a was used to fit the EIS data containing the Warburg impedance, and Fig.5b was utilized to the EIS data displaying only two capacitive loops[21]. The equivalent electrical circuits composed of the solution resistance (R_s) in series with a parallel combination of charge-transfer resistance (R_{ct}), surface resistance (R_f) and capacitance(Q_f), double-layer capacitance (Q_{dl}), and Warburg impedance (Z_w). The standard deviation, χ^2 , is order of $10^{-3} \sim 10^{-5}$.

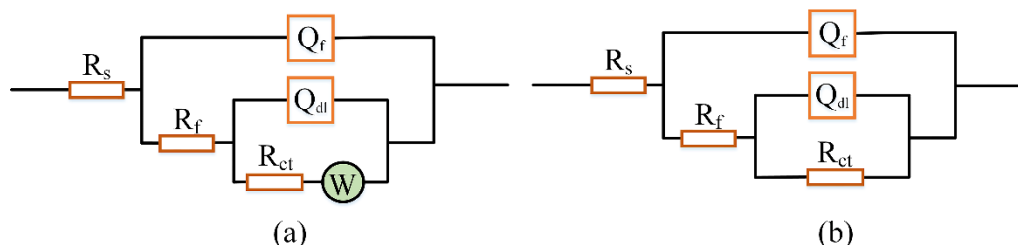


Figure 5. Equivalent electrical circuits (a) for fitting the data with the Warburg impedance (b) for fitting the data displaying two capacitive loops

The fitting parameters value in equivalents circuits are listed in the Table 2. R_{ct} reflects the corrosion rate determined by Faradaic process[16], and initial values decreases significantly both of two kinds of copper coins. Though group B possesses a larger resistance, it shows that the protective effect of BTA on the matrix decreases with the prolongation of immersion time at the initial stage, after which the values of R_{ct} experiences a remarkable growth. In contrast to the previous result, Group A shows better corrosion resistance because the impedance is as much as 50% higher than that of group B, which is consistent with the trend of weight gain results. (shown in Fig.2).

Table 2. Fitted impedance parameters for copper coins in synthetic sweat after different immersion time, obtained by using the EEC model describing in Fig.5. i.e. R_s , R_p , $R_{ct}[\Omega \cdot cm^2]$, Y_f , $Y_{dl}[\Omega \cdot cm^2 \cdot S^{-n}]$, $W[\Omega^{-1} \cdot S^{-1/2}]$

Samples	day	R_s	Q_f		R_f	Q_{dl}		R_{ct}	W	χ^2
			Y_f	n_f		Y_{dl}	n_{dl}			
GroupA	0	53.44	4.28E-04	0.614	1244.0	2.66E-02	1	1182.0	0.0037	1.29E-03
	1	48.37	6.58E-04	0.642	1060.0	2.03E-04	0.776	859.1	0.0086	3.64E-04
	3	48.69	1.14E-03	0.642	654.8	2.57E-04	0.7919	525.8	0.0176	2.58E-04
	5	49.26	1.94E-03	0.665	440.7	8.39E-02	0.8912	28.8	0.0131	2.03E-04
	7	46.89	3.35E-04	0.757	166.0	5.15E-02	0.7609	378.2	-	9.24E-04
	9	53.56	1.73E-04	0.888	53.2	1.14E-03	0.6808	1606.0	-	1.88E-04
	11	54.36	7.71E-07	0.909	113.2	1.50E-03	0.6534	2351.0	-	5.39E-04
GroupB	13	51.67	4.22E-07	0.925	157.0	1.86E-03	0.5945	3795.0	-	4.87E-04
	0	53.43	4.29E-04	0.800	1248.0	2.85E-02	0.89	2240.0	-	1.32E-03
	1	48.99	9.39E-04	0.620	1198.0	3.52E-02	1	566.8	-	6.87E-04
	3	49.22	1.48E-03	0.634	695.8	6.60E-02	0.8	417.1	-	4.15E-04

5	49.52	1.94E-03	0.666	437.9	8.20E-02	0.7804	262.7	-	2.07E-04
7	56.30	1.98E-03	0.713	299.7	4.41E-02	0.5546	300.7	-	1.78E-04
9	20.61	7.23E-04	0.224	87.1	6.97E-04	0.8298	1226.0	-	9.40E-05
11	64.10	1.68E-06	0.907	36.0	1.42E-03	0.6828	1503.0	-	3.36E-04
13	60.92	7.63E-07	0.935	51.6	1.57E-03	0.6381	2474.0	-	5.85E-04

3.3 Morphologies of corrosion products

Fig.6 exhibits the surface morphologies of corrosion products formed on copper coins coated with synthetic sweat after 240h of corrosion in accelerated environment. Whether group A or group B, the appearance of corrosion products on its surface is nubby structure, and cracks are clustered and loose; the surface is rough at high magnification, similar to the contour line in mountain areas, and there are plenty of gaps at the overlap of blocks. Corrosive media is easy to accumulate in cracks and voids, causing further corrosion. This reaction is the main factor of material loss and eventually the complete corrosion of the metal[18]. Although the final morphology of corrosion products is similar, there are still some differences in composition. Table 3 presents the EDS results of corrosion product. Both corrosion products in group A and group B contain Cu、Cl、O and Ni. In an environment with chloride ions, it is the most likely with existence of paratacamite ($Cu_2(OH)_3Cl$) on copper surface[14, 22]. In addition, corrosion products containing Zn were also detectable on copper coins coated BTA, which may explain higher corrosion rate of group B.

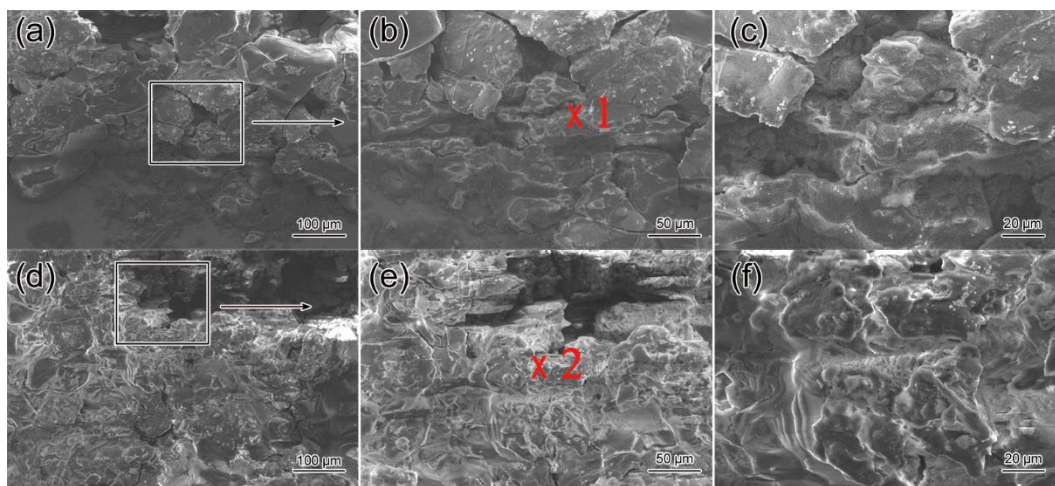


Figure 6. Surface morphology of corrosion products of copper coins coated with synthetic sweat after 240h in accelerated environment(a, b, c belong to Group A; d, e, f belong to Group B)

Table 3. Element contents of points marked in Figure 7 determined by EDS

Points	Cu(at%)	Ni(at%)	Zn(at%)	Cl(at%)	O(at%)
1	30.46	6.14	--	25.28	38.12
2	29.76	6.25	6.98	23.1	33.91

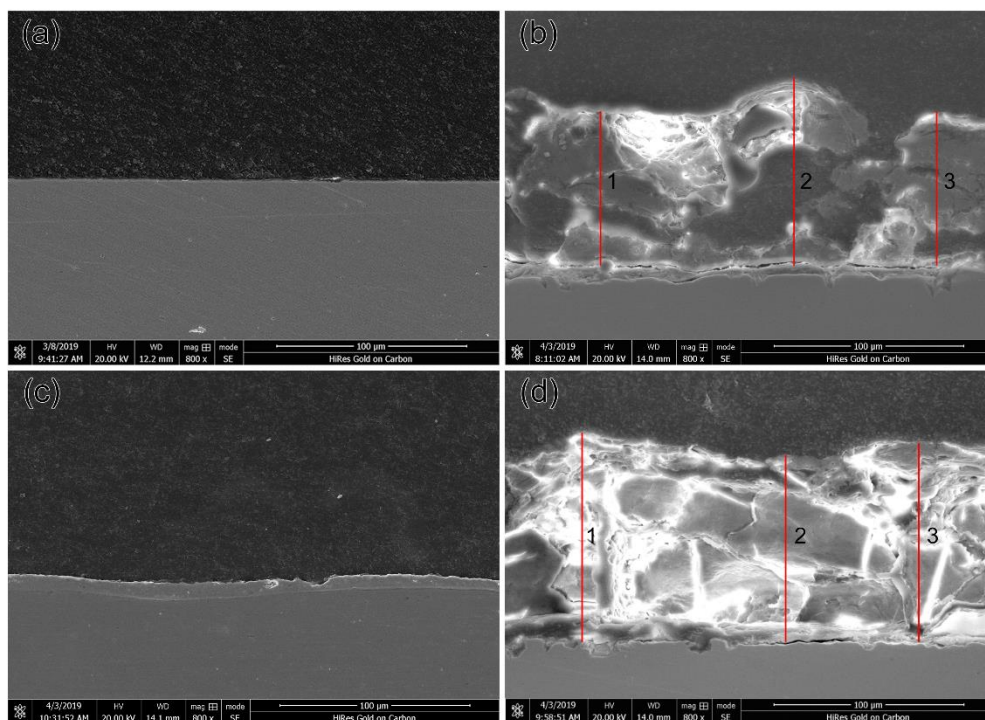


Figure 7. Cross-sectional morphology of copper coins: (a) initial sample of group A ; (b) corrosion product of group A; (c) initial sample of group B; (d) corrosion product of group B

Fig.7 presents the cross-sectional SEM images of copper coin substrate with or without BTA and corresponding corrosion products. The thickness of BTA-Cu film formed on copper coin substrate is about 6.2-9.1 μm , as indicated in Fig.7c. The labeling site’s composition of BTA-Cu is 52.5 at% C, 7.2 at % O, 6.6 at % Ni, 27.4 at % Cu, 6.2 at % Zn, which demonstrates that BTA not only reacts with Cu, but also complexes with Zn and Ni.

The thickness of the patina layer has been measured and the results are shown in the Table 4. The value of average thickness of the corrosion product in group B is higher than that in group A. If corrosion product can hinder reactants reaching sample surface, the corrosion rate will decrease with the accumulation of corrosion product[23]. However, it is clearly observed that corrosion products are porous. Corrosive substances easily penetrate into matrix through cracks and voids. In other words, BTA has little effect on inhibiting copper coin corrosion in synthetic sweat, even though it can promote the thickening of corrosion product layer.

The morphology of corrosion products can be compared horizontally and the corrosion depth can be analyzed vertically. It can be found that: (1) There will be more voids when the corrosion products accumulate on the surface. (2) The corrosion product layer of group B is well combined with the matrix.

Table 4. Thickness comparison of corrosion products of copper coins

Number	1	2	3	Average(μm)
Figure 7b	81.15	98.77	81.15	87.02
Figure 7d	110.10	98.49	104.53	104.38

It's revealed that the elements in the patina layer are heterogeneities from Fig.8 and 9. Since the porous structure of corrosion product facilitates the penetration of the epoxy resin and produces obvious fluorescence, quantitative analysis of carbon is not feasible[24]. But the density of corrosion product in this area can be roughly judged according to the content distribution of C element. As seen from Fig.8 b, the corrosion products of copper coins without BTA are loose as carbon penetrates the most of patina layer. The C element of corrosion product in group B remains a little content and uneven distribution. There still exists epoxy resin which diffused and aggregated through cracks. Although both corrosion products have cracks, the corrosion product layer of group B is relatively dense as a whole.

The composition of corrosion product is mainly metal chloride and there is no doubt that Cl element mainly concentrates in the patina layer. Compared with group A, it can be seen that the neat morphology and relatively abundant metal elements in corrosion products of group B (Fig.9 b), the complexation of BTA to Cu/Zn/Ni is quite obvious. It can be concluded that the main function of BTA is form the outer physical protective film[8], which can't provide effective protection for the matrix in the synthetic sweat.

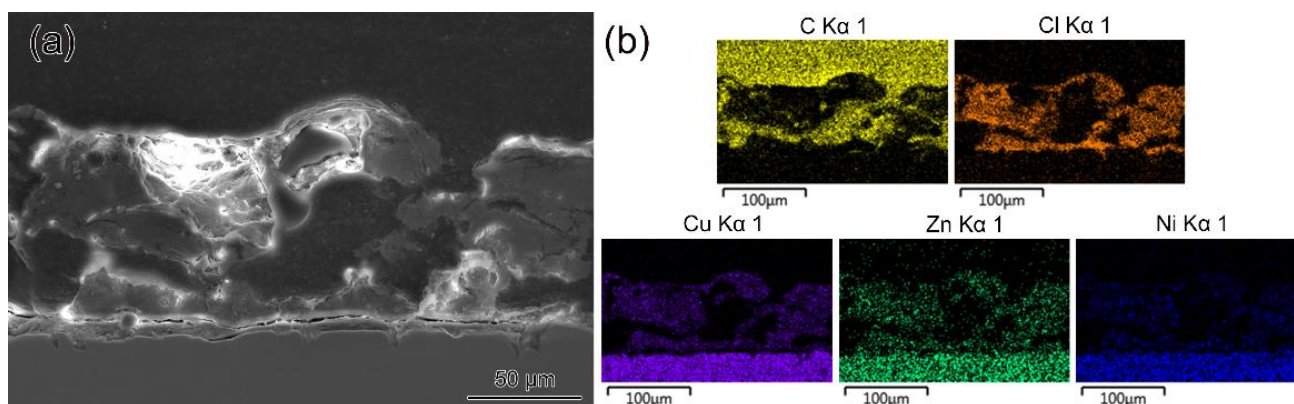


Figure 8. Copper coins of group A: (a) the area examined by SEM (SE mode); (b) elemental mapping of section a

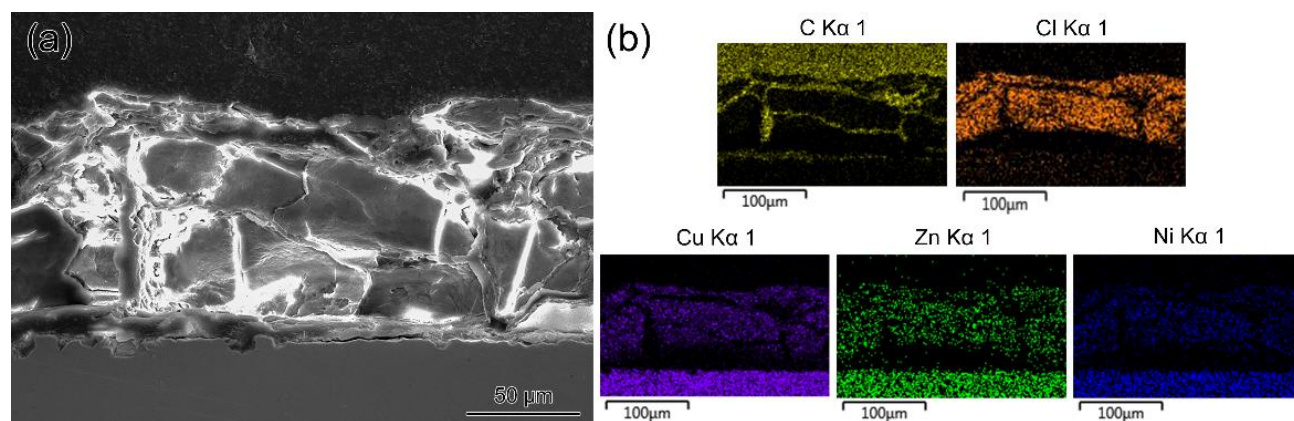


Figure 9. Copper coins of group B: (a) the area examined by SEM (SE mode); (b) elemental mapping of section a

3.4 Composition of corrosion products

Fig.10 is the XRD spectra of the corrosion products. It indicates that the main corrosion products formed on copper coins were identified as $\text{Cu}(\text{OH})\text{Cl}$ 、 $\text{Cu}_2(\text{OH})_3\text{Cl}$ and Cu_2NiZn , which is in agreement with precious literature on Cu-base alloys in synthetic sweat[14, 25-26]. Besides, NaCl can also be detected in the corrosion products, which is owing to the crystallization after synthetic sweat evaporation. The deposition amount of corrosion media on the surface is constant, and the presence of NaCl does not affect the comparison between the two groups of samples. However, the presence of corrosion products containing zinc and nickel was rarely detected by XRD. In order to further distinguish the composition of the corrosion products, XPS method was used.

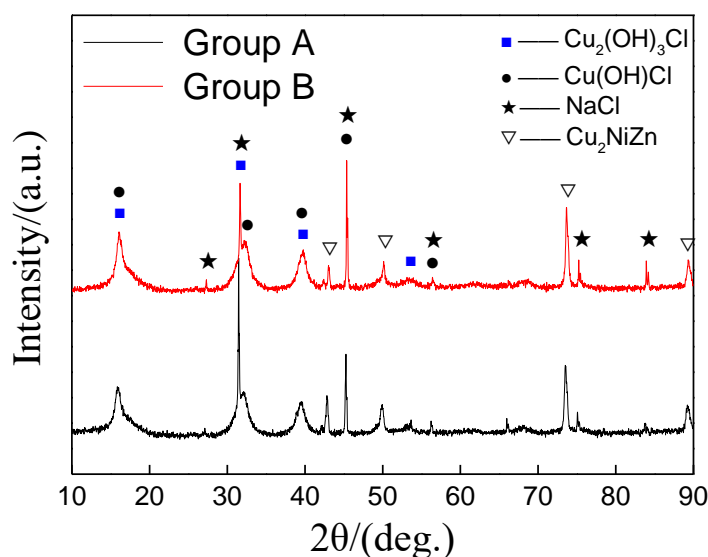


Figure 10. XRD patterns of corrosion products formed on copper coins coated with synthetic sweat after 240h of corrosion in accelerated environment

It's well known that process of copper oxidation is easy to adsorb polar contaminants[27-28]. Therefore, C 1s peak which reported currently at 284.5 eV[11-12] is only used for XPS spectra binding energy normalizations, and not used for analysis. Fig.11 and 12 show the XPS spectra of the corrosion products formed on copper coins. Five peaks including oxygen, chlorine, copper, zinc, nickel are observed in the XPS spectrum. The high resolution XPS spectra for O 1s, Cu 2p, Zn 2p and Ni 2p are illustrated in the following figure.

The O 1s peak at around 535.1eV, 531.7eV and 529.7eV respectively corresponds to the H_2O , $\text{Ni}(\text{OH})_2$ and CuO . As presented in Fig.11c. The Cu 2p spectrum includes two characteristic peaks, i.e. Cu 2p_{1/2} and Cu 2p_{3/2}. According to NIST standard database[11], Cu 2p_{1/2} and Cu 2p_{3/2} peaks for the CuO are seated at E_B of 952.70~953.70 eV and 933.6~934.2 eV. There are typical shake-up satellites in Cu 2p spectrum, indicating that the Cu(II) species exist in corrosion products[29-30]. Under the accelerated experiment of synthetic sweat, the probable substance of Cu (II) are copper oxide (CuO), copper chloride hydroxide($\text{Cu}_2(\text{OH})_3\text{Cl}$) and cupric chloride (CuCl_2), which is a supplement to the analysis of XRD and EDS. However, it can't be ruled out that the corrosion products contain copper (II)-BTA. The satellite peak is the energy loss peak caused by the electron relaxation process. In general, the

intensity of the satellite peak is about 5% - 10% of the main peak[31]. As shown in Fig.11d, the peak of Zn 2p can be divided into 1023.1eV (ZnCl₂ 2P_{3/2}) and 1021.2ev (ZnO 2p_{3/2} or Zn 2p_{3/2}). Corresponding to the chloride/oxide of zinc, it is shown that some zinc ions exist in the corrosion product as chloride/oxide.

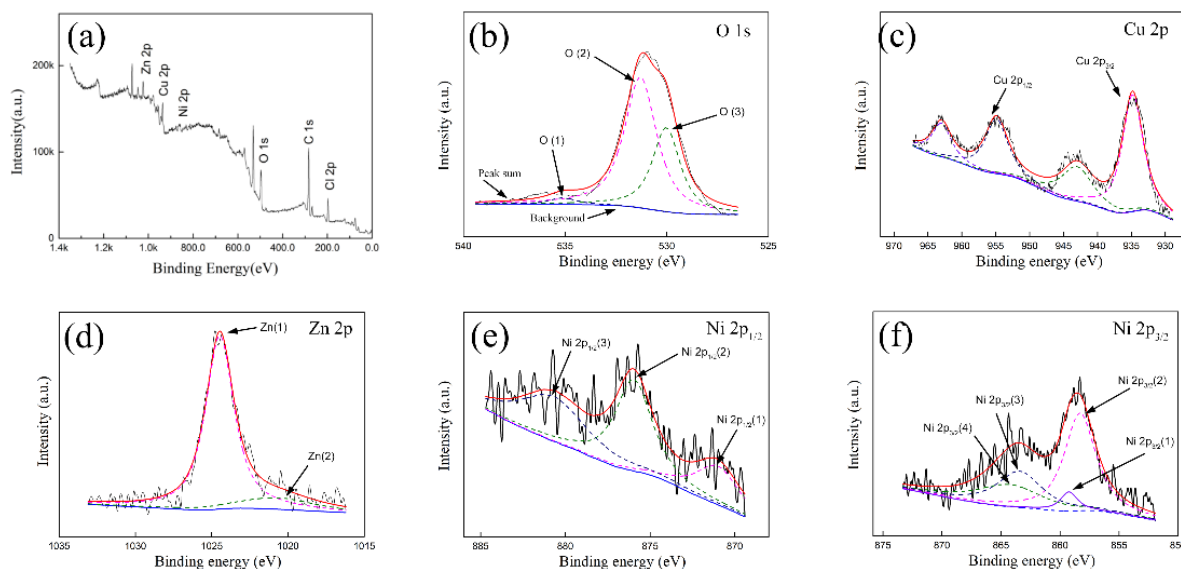


Figure 11. (a) XPS overview spectrum and deconvolution spectra of (b) O 1s, (c) Cu 1s, (d) Zn 2p, (e) Ni 2p 1/2 and (f) Ni 2p 3/2 elements detected on corrosion products of group A smeared with artificial sweat after 240 h in accelerated environment.

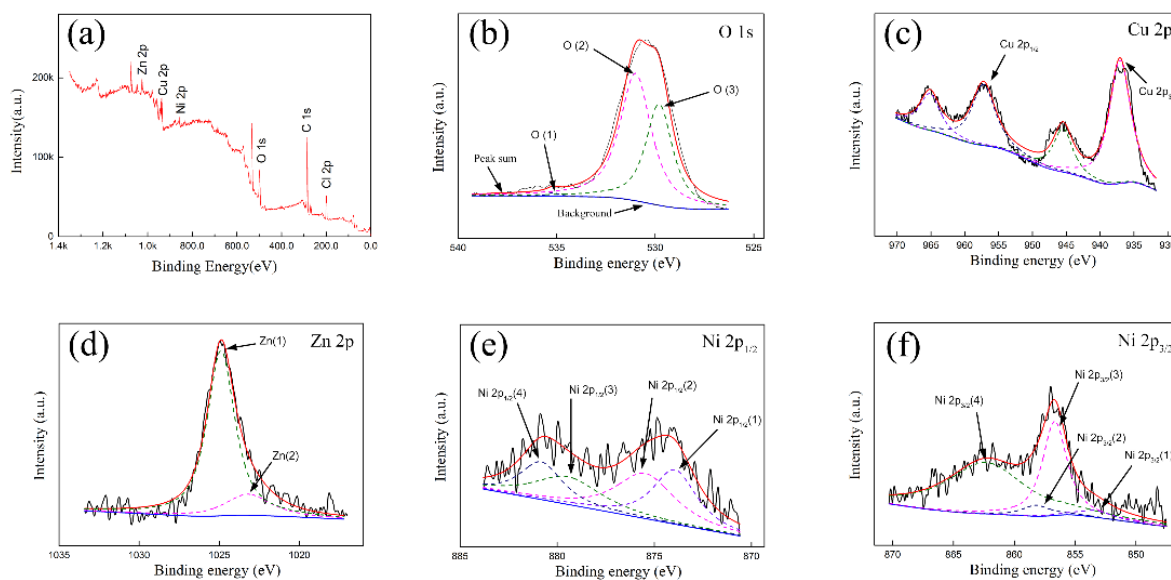


Figure 12. (a) XPS overview spectrum and deconvolution spectra of (b) O 1s, (c) Cu 1s, (d) Zn 2p, (e) Ni 2p 1/2 and (f) Ni 2p 3/2 elements detected on corrosion products of group B smeared with artificial sweat after 240 h in accelerated environment.

Moreover, Ni 2p (shown in Fig.11 e-f) can be separated into two main peaks, Ni 2p_{1/2} and Ni 2p_{3/2} correspond to 873.8eV and 855.02 eV respectively[32], and there is another energy loss peak in front of the satellite peak. There are two satellite peaks at about 881.8 eV and 864.1 eV, which are characteristic of nickel oxides. Furthermore, the peaks at about 874.97 eV, 858.31eV and 861.7 eV indicate the presence of the nickel and nickel hydroxide.

The XPS spectra of BTA-treated copper coins after 240h of corrosion synthetic sweat accelerated corrosion are shown in Fig.12. The characteristic peaks of Cu and Zn are basically similar, which also enhances the reliability of the components detected by XRD spectra. It can also be divided into two main peaks in Fig.12 e-f, Ni 2p_{1/2} and Ni 2p_{3/2}, respectively. The corrosion products containing nickel are mainly Ni/NiO/Ni(OH)₂, but their contents may be different from those of group A.

3.5. Discussion

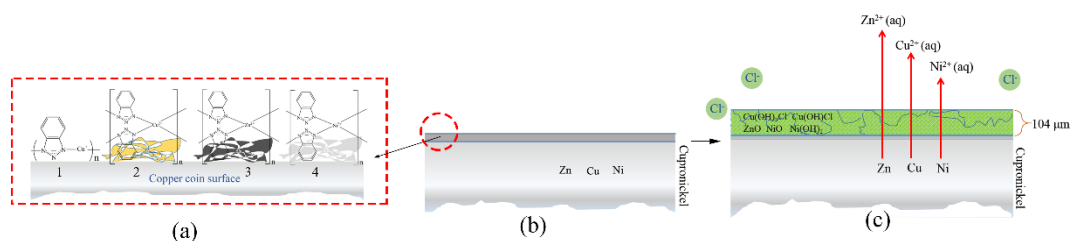
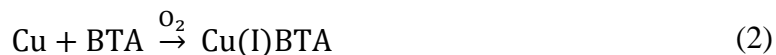


Figure 13. Schematic diagram of corrosion process (a) several inhibition mechanisms between BTA molecules and metal cations: 1. Cu(I)-BTA 2. Cu(II)-BTA 3.Zn(II)-BTA 4.Ni(II)-BTA (b) initial sample of group B (c) corrosion sample of group B

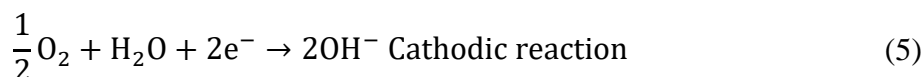
The corrosion evolution of copper-coin coated with BTA under synthetic sweat is briefly shown in Fig.13 based on the electrochemical performance and the surface analysis. BTA is a heterocyclic compound which functions by chemical bonding on the surface of metal or metal oxide. Therefore, the metal surface layer will be composed of both oxide and polymer components[33]. Several inhibition mechanisms between BTA molecules and metal cation are shown in the Fig.13a. The interaction models between BTA and copper are based on Eq. (2) to produce Cu(I)-BTA [34-35] and Eq. (3) to produce Cu(II)-BTA[13, 36]. It has been reported that Co(II) -BTA exists[37], and Ni and Zn are adjacent elements in the same period as copper. In addition, cross-section analysis shows that the composition of BTA complex contains Zn and Ni. Therefore, it is possible that BTA molecules also interacts with Zn²⁺/Ni²⁺ cations, leading chelate formation of Zn(II)-BTA and Ni(II)-BTA on the surface.



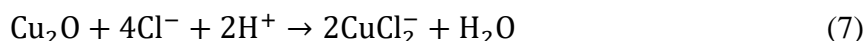
In synthetic sweat solution, the protective film is preferentially corroded. High chloride concentration will reverse the chemical equilibrium. The participation of chloride ions in acidic environment will release metal ions from the binding of BTA, such as Cu²⁺, Ni²⁺ and Zn²⁺, and promote more metal ions to react with corrosive media. The existence of NiO/Ni(OH)₂ and ZnCl₂/ZnO was

detected from the XPS spectra in corrosion products. In other words, the corrosion behavior of the protective film is accelerated. It is a reason why the weight of corrosion product gains more.

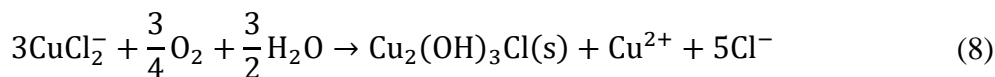
At the initial corrosion stages of group A, there were only a few corrosion products on the surface of copper coins. Copper corrosion was mainly influenced by oxygen diffusion as the anodic reaction was slow[38]. $\text{Cu}_2(\text{OH})_3\text{Cl}$ appeared in all samples after cyclic test (wet and dry, 240h). The corrosion behavior of copper coins in synthetic sweat can be regarded as corrosion under chloride-containing thin electrolyte layers. Electrochemical corrosion occurred on the surface according to Eq. (4-5).



Relied on pH and chloride concentration, the Cu^+ ions produced by anodic reaction will be converted into nanokite or cuprite, and the chloride ions resulted in the breakdown of passive Cu_2O film on the copper surface to form soluble species, such as CuCl or CuCl_2^- [39].



The anodic dissolution is determined by the transfer rate of CuCl_2^- from the copper surface to liquid film[38]. The CuCl_2^- formed will be further oxidized to copper hydroxychloride and copper(II) chloride in air[40] according to Eq. (8). It is also the reaction pathway of group B patina in the synthetic sweat.



4. CONCLUSIONS

(1) Under the condition of alternating wetting and drying, the surface of copper coins protected by BTA will generate more loose green patina. The reason for the difference of corrosion is that the BTA-Metal complex is more sensitive to solution corrosion medium. As the small ionic radius, it is easy for chloride ion to adsorb strongly with metal surface, which may destroy the chemical bond between BTA and metal ion, and the impedance value of the sample will decrease.

(2) The composition of BTA film is composed of Cu, Zn and Ni. One possible reason is that BTA not only binds to Cu, but also to Ni and Zn. BTA has no effect on the composition of the final corrosion products. Its main components are $\text{Cu}_2(\text{OH})_3\text{Cl}$ 、 $\text{NiO/Ni}(\text{OH})_2$ and ZnCl_2/ZnO . Compared with the blank group, copper coins coated BTA gain more weight in corrosion products. The chemical bond between BTA and metal ions will be broken eroded by synthetic sweat, and the released cation will react more easily with corrosive media. It can give a reliable explain to the difference of kinetic curves.

ACKNOWLEDGEMENTS

This work was supported by National Natural Science Foundation of China (No. 51671197) and Shenyang Mint Co.,Ltd

References

1. L. He, J.Y. Liang, X. Zhao and B.L. Jiang, *Microchem. J.*, 99 (2011) 203.
2. D.Q. Xia, Y. Qin, Z.W. Mao, P.J. Jin and Y.W. Dong, *Corros. Sci. Prot. Technol*, 22 (2010) 234.
3. N. Montoya, E. Montagna, Y. Lee, M. Teresa Domenech-Carbo and A. Domenech-Carbo, *J. Raman Spectrosc.*, 48 (2017) 1337.
4. R.H. Yao and J. Yang, *Journal of Southern Institute of Metallurgy* 000 (1997) 16.
5. C. Gattinoni, P. Tsaousis, C. Euaruksakul, R. Price, D.A. Duncan, T. Pasca, D. Prendergast, G. Held and A. Michaelides, *Langmuir*, 35 (2019) 882.
6. Z.B. Gu, Y.L. Liu, B.H. Gao, C.W. Wang and H.W. Deng, *Journal of Semiconductors*, 36 (2015) 6
7. Z.Y. Chen, L. Huang, G.A. Zhang, Y.B. Qiu and X.P. Guo, *Corros. Sci.*, 65 (2012) 214.
8. D. Gopi, E.M. Sherif, M. Surendiran, D.M.A. Sakila and L. Kavitha, *Surf. Interface Anal.*, 47 (2015) 618.
9. ISO 3160-2:2015(E), Watch-cases and accessories (Gold alloy coverings) Part 2: Determination of fineness, thickness, corrosion resistance and adhesion, Switzerland, 2015.
10. J.H. Scofield, *J. Electron. Spectrosc. Relat. Phenom.*, 8 (1976) 129.
11. V.N. Alexander, K.V. Anna, W.G. Stephen and J.P. Cedric, NIST Standard Reference Database 20, Version 4.1, 2012.
12. F.M. John and F.S. William, Handbook of X-ray photoelectron spectroscopy, Physical Electronics, (1992) Eden prairie, USA.
13. C.X. Yi, B.F. Zhu, Y. Chen, X.Q. Du, Y.M. Yang, J. Liu and Z. Zhang, *Sci. Rep.*, 8 (2018) 15.
14. J. Porcayo-Calderon, R.A. Rodriguez-Diaz, E. Porcayo-Palafox and L. Martinez-Gomez, *Journal of Chemistry*, (2016) 11.
15. Y. Zhang and Y. Chen, *Corros. Eng. Sci. Techn*, 54 (2019) 75.
16. G. Zerjav and I. Milosev, *Corros. Sci.*, 98 (2015) 180.
17. P. Mourya, P. Singh, R.B. Rastogi and M.M. Singh, *Appl. Surf. Sci.*, 380 (2016) 141.
18. M. Albin, P. Letardi, L. Mathys, L. Brambilla, J. Schroeter, P. Junier and E. Joseph, *Corros. Sci.*, 143 (2018) 84.
19. G. Zerjav and I. Milosev, *Materials and Corrosion-Werkstoffe Und Korrosion*, 67 (2016) 92.
20. C.N. Cao and J.Q. Zhang, An Introduction to Electrochemical Impedance Spectroscopy, Science Press, (2002) Beijing, CHINA.
21. C. Pan, M.X. Guo and Z.Y. Wang, *J. Mater. Eng. Perform.*, 28 (2019) 2562.
22. G. Di Carlo, C. Giuliani, C. Riccucci, M. Pascucci, E. Messina, G. Fierro, M. Lavorgna and G.M. Ingo, *Appl. Surf. Sci.*, 421 (2017) 120.
23. Y. Xiang, Z. Wang, Z. Li and W.D. Ni, *Corrosion*, 69 (2013) 251.
24. M. Serghini-Idrissi, M.C. Bernard, F.Z. Harrif, S. Joiret, K. Rahmouni, A. Srhiri, H. Takenouti, V. Vivier and M. Ziani, *Electrochim. Acta*, 50 (2005) 4699.
25. S. Colin, E. Beche, R. Berjoan, H. Jolibois and A. Chambaudet, *Corros. Sci.*, 41 (1999) 1051.
26. C.H. Liang, S.S. Wang, N.B. Huang and P. Wang, *T. Nonferr.Metal.Soc*, 25 (2015) 654.
27. M. Finsgar, *Corros. Sci.*, 72 (2013) 90.
28. P.E. Laibinis, Whitesides G. M., Allara D. L., Tao Y. T., Parikh A. N., Nuzzo R. G., *J. Am. Chem. Soc.*, 113 (1991) 7152.
29. M.C. Biesinger, L.W. Lau, A.R. Gerson and R.S. Smart, *Appl. Surf. Sci.*, 257 (2010) 887.
30. C.C. Chusuei, M.A. Brookshier and D.W. Goodman, *Langmuir*, 15 (1999) 2806.
31. J.Q. Wang, W.H. Wu and D.M. Feng, Introduction to Electron Spectroscopy (XPS, XAES, UPS), National Defence Industrial Press, (1992) Beijing, China.
32. I. Milogev and T. Kosec, *Electrochim. Acta*, 52 (2007) 6799.
33. T. Kosec, I. Milosev and B. Pihlar, *Appl. Surf. Sci.*, 253 (2007) 8863.
34. M. Finsgar and I. Milosev, *Corros. Sci.*, 52 (2010) 2737.

35. M.J. Kao, F.C. Hsu and J.B. Guo, *Current Applied Physics*, 13 (2013) S79.
36. G. Xue and J.F. Ding, *Appl. Surf. Sci.*, 40 (1990) 327.
37. H. Akhavan, M. Izadi, I. Mohammadi, T. Shahrabi and B. Ramezanzadeh, *J. Electrochem. Soc.*, 165 (2018) 670.
38. X.N. Liao, F.H. Cao, L.Y. Zheng, W.J. Liu, A.N. Chen, J.Q. Zhang and C.N. Cao, *Corros. Sci.*, 53 (2011) 3289.
39. P. Yi, C. Dong, K. Xiao and X. Li, *Appl. Surf. Sci.*, 399 (2017) 608.
40. H.J. Huang, Z.Q. Wang, Y.L. Gong, F. Gao, Z.P. Luo, S.T. Zhang and H.R. Li, *Corros. Sci.*, 123 (2017) 339.

© 2020 The Authors. Published by ESG (www.electrochemsci.org). This article is an open access article distributed under the terms and conditions of the Creative Commons Attribution license (<http://creativecommons.org/licenses/by/4.0/>).